Chemical-looping combustion and chemical-looping with oxygen uncoupling of kerosene with Mn- and Cu-based oxygen carriers in a circulating fluidized-bed 300 W laboratory reactor

Patrick Moldenhauer[a,*], Magnus Rydén[a], Tobias Mattisson[a], Anders Lyngfelt[a]

[a]*Department of Energy and Environment, Division of Energy Technology, Chalmers University of Technology, S-412 96 Göteborg, Sweden*

Abstract

The fuel conversion properties of two oxygen carriers, based on manganese- and copper-oxide, were investigated with sulphur-free kerosene in a chemical-looping reactor with continuous particle circulation. An injection system was used, in which kerosene was evaporated, mixed with superheated steam and fed directly into the lab scale chemical-looping reactor. The manganese-based oxygen carrier M4MZ-1200 was composed of 40 wt% Mn_3O_4 and 60 wt% MgO-ZrO_2 and was used for chemical-looping combustion (CLC) experiments for 17 h. The copper-based oxygen carrier C2Z-1050 was composed of 20 wt% CuO and 80 wt% ZrO_2 and was used for 45 h with fuel addition. With M4MZ-1200 oxygen carrier, 83 – 99.3 % of the fuel carbon was converted to CO_2 at temperatures between 800 °C and 950 °C and fuel flows equivalent to 144 – 462 W_{th}. Higher conversions at lower temperatures than with M4MZ-1200 were achieved with C2Z-1050, which is likely due to the ability of CuO to release gas phase oxygen in the fuel reactor, *i.e.* CLOU properties. Here, 99.99 % CO_2 yield was achieved at 900 °C and 144 W_{th} fuel equivalent. The particles were analyzed before and after the experiments using XRD, SEM, BET surface area and particle size distribution. Whereas nearly the whole batch of M4MZ-1200 particles was disintegrated after the experiments, only about 5 % of the C2Z-1050 particles turned to fines. This is the first time that combustion of liquid fuel using CLOU is demonstrated in a continuous unit.

Keywords: chemical-looping combustion (CLC), chemical-looping with oxygen uncoupling (CLOU), liquid fuel, manganese-based oxygen carrier, copper-based oxygen carrier, CO_2 capture

1. Introduction

This study focuses on the direct use of liquid fuel in a continuous chemical-looping process. It is part of a project with the final goal of utilizing heavy oil residues for heat and power production.

Both chemical-looping combustion and chemical-looping with oxygen uncoupling were conducted in a 300 W circulating fluidized-bed laboratory reactor.

1.1. Chemical-Looping Combustion

Chemical-looping combustion (CLC) is a method of burning fuels with inherent separation of CO_2 [1]. In the most common CLC approach, particles are circulated between two interconnected reactors, the air reactor and the fuel reactor, with no gas leakage between the reactors. In the air reactor (AR), the particles are oxidized with air, and in the fuel reactor (FR), they are reduced by fuel before the cycle begins anew. As the oxygen carrier (OC) is circulated between air and fuel reactors, it transports oxygen from air to fuel. Thus, air and fuel are never mixed and after condensing water, the stream of flue gases consists of nearly pure CO_2. An energy intensive gas separation is thus avoided. High efficiency, high CO_2 capture rate and the possibility to use different kinds of fuels suggests that CLC could be economically feasible and thus competitive.

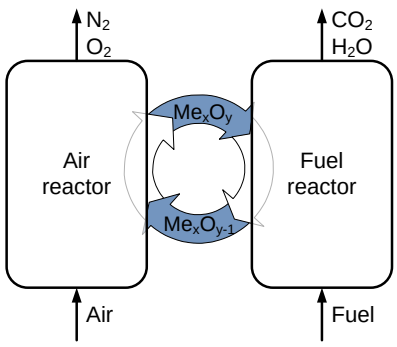

Figure 1: Schematic illustration of chemical-looping combustion

Figure 1 shows the basic design of a CLC system and illustrates the working principle. The reactions in air reactor and fuel reactor are expressed by reactions (1) and (2).

$$\text{AR:} \qquad Me_xO_{y-1} + {}^1/_2\,O_2 \longrightarrow Me_xO_y \tag{1}$$

$$\text{FR:} \qquad (2n+m)\,Me_xO_y + C_nH_{2m} \longrightarrow (2n+m)\,Me_xO_{y-1} + m\,H_2O + n\,CO_2 \tag{2}$$

*Corresponding author. *Telephone:* +46 (0)31-772 1469
Email address: patrick.moldenhauer@chalmers.se (Patrick Moldenhauer)

Here Me_xO_y denotes a metal oxide. The oxidation of particles in the air reactor, see reaction (1), is exothermic. The reducing reaction in the fuel reactor, see reaction (2), can be either exothermic or endothermic, depending on oxygen carrier material and fuel used.

Results have been published from twelve operational continuous chemical-looping combustors with thermal capacities ranging from 300 W to 140 kW and a total operational experience of more than 4000 h [2]. The majority these experiments were performed with gaseous fuel, methane, natural gas or syngas, followed by solid fuels. Liquid fuels have been examined in laboratory batch experiments [3–8] and in continuous operation [9]. A throughout discussion of the mentioned publications can be found in an earlier work by the authors [9].

1.2. Chemical-Looping Combustion with Oxygen Uncoupling

Chemical-looping combustion with oxygen uncoupling (CLOU) is a variation of chemical-looping combustion. After oxidation of the oxygen carrier in the air reactor according to reaction (1), the oxidized oxygen carrier is transported into the fuel reactor, where it releases oxygen in gaseous form, see reaction (3). Reactions between fuel and gas-phase oxygen, see reaction (4), are much likely faster than the corresponding CLC reaction, see reaction (2), where fuel reacts with oxygen that is bound to the solid oxygen carrier.

$$Me_xO_y \longrightarrow Me_xO_{y-1} + {}^1\!/_2\, O_2(g) \qquad (3)$$

$$C_nH_{2m} + (n + {}^1\!/_2\, m)\, O_2 \longrightarrow m\, H_2O + n\, CO_2 \qquad (4)$$

The typical mechanism for oxygen release, as shown in reaction (3), is a phase change of the oxygen carrier between air reactor and fuel reactor. The phase change in turn is triggered by a change in temperature and/or oxygen concentration. Whether or not a CLC process is also a CLOU process is determined by the properties of the oxygen carrier, *i.e.* its ability to release gas phase oxygen under prevailing conditions.

Reactions between two solids, as in CLC with solid fuels, are potentially slow. The use of an oxygen carrier with CLOU properties in combination with solid fuel is thus beneficial. But even for gaseous and liquid fuels the use of a CLOU material is expected to show a clear improvement in fuel conversion for three reasons.

1. In a well-mixed bed there will be oxygen released at the top of the bed, which can oxidize gas that bypasses the bed in bubbles, and hence it is very likely that much less oxygen carrier material will be needed in order to fully convert the fuel.
2. If the oxygen release is rapid, as has been seen previously with CuO material [10], the overall reaction will be governed by the normal combustion reaction, which is likely more rapid than the gas-solid reaction occuring in regular CLC.
3. In CLC and for a first order reaction, the gas yield as a function of bed mass can be expected to approach full conversion asymptotically, meaning much higher relative bed masses will be needed to convert the last remnants of the fuel [11]. This is not the case with CLOU in a fluidized bed, where the oxygen release is in principle independent of gaseous reactant concentration. Thus, the bed mass needed to reach full conversion of fuel is potentially much lower with CLOU as compared to regular CLC.

The CLOU concept was proposed by Lyngfelt and Mattisson in 2005 [12]. The first experiments in a batch reactor with solid fuels are described in [10, 13]. A detailed description of the CLOU concept can be found in [14].

2. Experimental Details

2.1. 300 W Laboratory Reactor

The working principle of the reactor, which was used for the experiments in this work, is shown in Figure 2. The reactor is 300 mm high. The fuel reactor has a cross-section of 25 mm × 25 mm. The base of the air reactor is 25 mm × 42 mm and contracts to 25 mm × 25 mm in the riser section. Fuel and air enter the system through separate windboxes, located in the bottom of each reactor. Porous quartz plates act as gas distributors. In the air reactor, the gas velocity is sufficiently high to create a circulating fluidized bed and oxygen carrier particles are thrown upwards. The particle-gas mixture is then separated: oxygen depleted air is returned to the atmosphere, whereas a fraction of particles falls into the standpipe of the downcomer, which is the inlet of a J-type loop-seal. From the loop-seal, particles overflow into the fuel reactor via the return orifice. The fuel reactor is a bubbling bed reactor. From the bottom of the fuel reactor, particles flow into the underflow standpipe of the slot, which is essentially a J-type loop-seal, and return to the air reactor, where the whole cycle starts over again.

The exit pipe of the fuel reactor is connected to a water seal with a column height of 1 – 2 cm. As a result, the pressure in the fuel reactor is 0.1 – 0.2 kPa higher than in the air reactor, which reduces gas leakage from air reactor to fuel reactor.

Metal oxide particles in the air reactor are fluidized with air, and reduced particles (Me_xO_{y-1}) are oxidized according to reaction (1). In the fuel reactor the metal particles are fluidized by gas-phase fuel or, in case of kerosene, a gaseous steam-fuel mixture. Particle reduction occurs either directly by fuel, according to reaction (2), or, if a CLOU oxygen carrier is used, indirectly through oxygen released, see reaction (3).

The 300 W reactor is subject to high heat losses due to a high surface-to-volume ratio. In order to achieve sufficiently high temperatures, typically 750 – 950 °C, the reactor is encased in an electric furnace.

2.2. Fuel

The fuel was kerosene, which was provided by courtesy of Preem AB in Gothenburg, Sweden. By definition kerosene consists of different hydrocarbons with evaporation temperatures between 150 °C and 320 °C. An elemental analysis showed a composition of 86.2 wt% carbon and 13.5 wt% hydrogen, which corresponds to a molar hydrogen-to-carbon ratio H/C of 1.88.

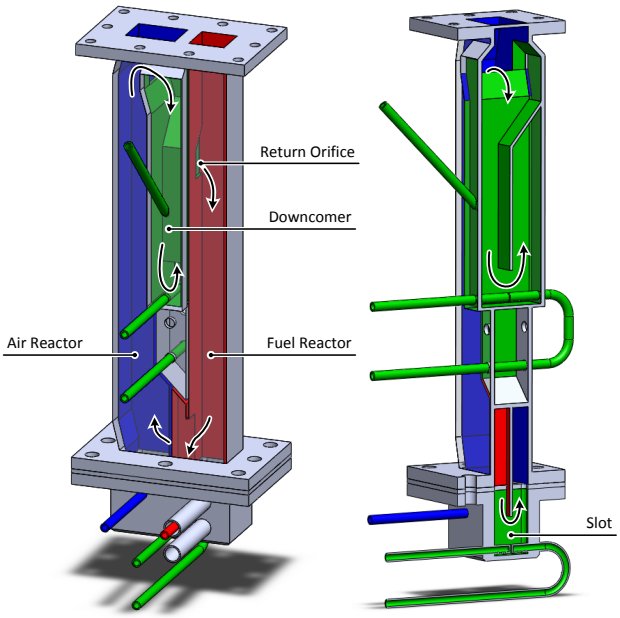

Figure 2: Schematic three-dimensional illustration of the 300 W laboratory reactor

The lower heating value was determined to be 43.34 MJ/kg. It is likely that the fuel not only contains linear alkanes but also branched iso-alkanes and possibly cyclic alkanes. The elemental analysis suggests the presence of arenes. Alkenes and alkynes are rather unlikely in mineral oil.

The fuel was also analyzed in a gas chromatograph (GC) with the simulated distillation method according to ASTM standard D-2887-08, which is a standard test method for boiling range distribution of petroleum fractions. It was found that 99 wt% of the fuel content has an evaporation point below 250 °C and 80 wt% below 200 °C. Some of the peaks in the analysis coincided with those of linear alkanes. The most prominent ones were n-C10 (H/C = 2.20; T_{boil} = 174 °C) and n-C11 (H/C = 2.18; T_{boil} = 196 °C).

2.3. Injection Principle

The injection system was constructed and tested using the 300 W chemical-looping reactor, see Figure 2. The basic principle behind the injection system is to evaporate the liquid fuel using superheated steam as heat source and to inject the resulting steam-fuel gas mixture into the fuel reactor. This is most convenient, because it causes the least changes to the reactor system, which is designed for gaseous fuels.

When the fuel molecules are converted the gas volume will increase. Hence, the volume flow of the gaseous steam-fuel mixture is a function of the extent of hydrocarbon converted. The steam fulfils the secondary function of ensuring that enough gas is available to fluidize the particles in the fuel reactor. Poorly fluidized particles increase the risk of agglomeration, which may destroy the oxygen carrier batch, depending upon the type of material used.

Figure 3 shows how evaporation, mixing and injection are realized. Steam is generated continuously by a steam generator. A heating band is used to superheat the steam to the desired temperature, which is measured by a thermocouple temperature sensor. A continuous fuel flow is provided by a diaphragm metering pump. The fuel is fed through a capillary tube, which is concentrically arranged within the steam pipe. The heat necessary for evaporation of the fuel is thereby transported from steam to fuel.

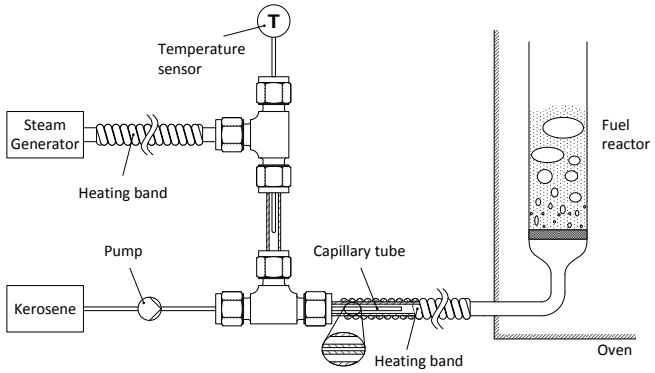

Figure 3: Schematic illustration of the injection principle for kerosene injection

2.4. Measurements

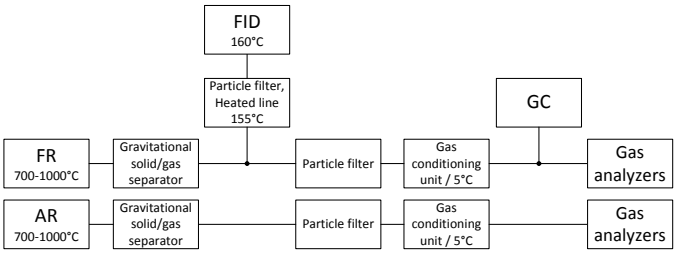

Figure 4: Schematic measurement layout

Figure 4 shows a schematic of the downstream gas measurements. The top part of the 300 W reactor is connected to a gravitational solid / gas separator, one for the air reactor and one for the fuel reactor. Part of the hot flue gases of the fuel reactor are diverted and led through a heated line, at 155 °C, to a flame ionization detector (FID). The FID measures the content of organic carbon as a CH_4 equivalent, without giving information about aromaticity or hydrogen content. The flue gases of both air reactor and fuel reactor are separately filtered and cooled down to 5 °C, before they pass through gas analyzers. The dry-gas content of CH_4, CO and CO_2 is measured continuously by an IR analyzer and the content of O_2 by a paramagnetic sensor. Additionally, the dry fuel reactor gas is intermittently analyzed in a gas chromatograph (GC), which measures, besides the previously mentioned gases, H_2, N_2, and hydrocarbons up to C_3H_8. The GC used is equipped with two columns, Molsieve MS5Å 10 m × 0.32 mm (ID) and PoraPLOT Q 10 m × 0.15 mm (ID), in which the gas sample is injected in parallel.

In addition to the analysis of in situ data, XRD measurements, density measurements and measurements of the BET surface area (through gas adsorption) were performed with particles before and after the experiments.

2.5. Oxygen Carriers

Two oxygen carriers were used for the experiments, manganese-based M4MZ-1200 and copper-based C2Z-1050. Both oxygen carrier materials consist of an active part, manganese oxide and copper oxide respectively, and an inert part, zirconium dioxide. Mixing active and inert material is a compromise between oxygen carrier reactivity and lifetime. M4MZ-1200 consists of 40 wt% Mn_3O_4 supported on 60 wt% ZrO_2, which was partially Mg-stabilized. C2Z-1050 consists of 20 wt% CuO supported on 80 wt% ZrO_2. Both particle types were produced through spray-drying with subsequent calcination at 1200 °C and 1050 °C respectively. The particles were supplied by VITO NV, Flemish Institute for Technological Research.

The oxygen carriers M4MZ-1200 and C2Z-1050 have oxygen transfer capacities of 2.8 wt% and 2.0 wt%, see Table 1. Whereas MnO cannot be reduced to Mn under typical CLC conditions [15], a transition from Cu_2O to Cu is possible. This might not always be desirable, because metallic copper has a low melting point and can thus form agglomerations.

Table 1: Oxidation states and oxidation transfer capacity of manganese-based oxygen carrier M4MZ-1200 and copper-based oxygen carrier C2Z-1050

Short name	Oxidized state	Reduced state	R_o (%)
M4MZ-1200	Mn_3O_4 + MgO-ZrO_2	MnO + MgO-ZrO_2	2.8
C2Z-1050	CuO + ZrO_2	Cu_2O + ZrO_2	2.0

A freeze granulated material similar to M4MZ-1200 has been investigated previously in both a batch reactor [16] and the 300 W unit [17] using syngas and natural gas as fuel. In those experiments the particles showed high fuel conversion, albeit lower than those of nickel-based oxygen carriers. No issues regarding agglomeration and fluidization were noted.

Different copper-based particles have been used in earlier studies [10, 13, 18–22]. The results were generally very promising. Copper-based oxygen carriers are known to have good conversion capabilities for solid fuels, which can be attributed by the so called CLOU effect, *i.e.* the release of gas-phase oxygen in the fuel reactor. Due to the rather low melting point of metallic copper, which can be formed during reduction, high temperatures sometimes cause agglomeration of the oxygen carrier particles.

The reactor was filled with 350 g of M4MZ-1200 in the size range of 90 – 212 µm for the experiments with manganese-based oxygen carrier. 310 g of C2Z-1050 in the size range of 90 – 250 µm were used for the experiments with copper-based oxygen carrier.

2.6. Conducted Experiments

Chemical-looping combustion experiments were conducted with temperatures between 650 °C and 950 °C and fuel flows corresponding to 144 – 462 W_{th}. The amount of added steam was constant for all fuel flows and 0.75 ml_{liq}min. The parameters for the different experiments are summarized in Table 2.

M1 – M3 and C2 – C7 in Table 2 are combustion experiments with manganese-based oxygen carrier and copper-based oxygen carrier respectively. C1 and C8 were performed without fuel addition. Instead, oxygen release, *i.e.* CLOU, properties of fresh and used particles were tested. Chemical-looping experiments with M4MZ-1200 and C2Z-1050 under fuel addition were performed for about 17 h and 45 h respectively.

3. Data Evaluation

3.1. Fuel Combustion

With the current measurement system only carbon is measured thoroughly. Hydrogen is only measured in pure form or in the form of hydrocarbons up to C_3H_8. Due to this circumstance the evaluation of the combustion process will be based on the fate of carbon. The fractions of exiting carbon species are related to the flow of carbon into the fuel reactor. These are listed in Table 3 and the corresponding calculations are given in equations (5) – (9).

$$C_{AR} = \frac{\dot{n}_{CO2,AR}}{\dot{n}_{C,fuel,in}} \tag{5}$$

$$C_{CO2,FR} = \frac{\dot{n}_{CO2,FR}}{\dot{n}_{C,fuel,in}} \tag{6}$$

$$C_{CO,FR} = \frac{\dot{n}_{CO,FR}}{\dot{n}_{C,fuel,in}} \tag{7}$$

$$C_{CH4,FR} = \frac{\dot{n}_{CH4,FR}}{\dot{n}_{C,fuel,in}} \tag{8}$$

$$C_{>CH4,FR} = \frac{\sum_{m=1}^{9}(m \cdot \dot{n}_{CmHn,FR}) - \dot{n}_{CH4,FR}}{\dot{n}_{C,fuel,in}} \tag{9}$$

$\dot{n}_{C,fuel,in}$ is the total molar flow of carbon into the reactor with kerosene and $\dot{n}_i$ is the molar flow of species i exiting the reactor. This way of evaluating the combustion process is possible by drawing a mass balance around the reactor system as a whole, *i.e.* air reactor and fuel reactor. A more compact way of evaluating the combustion process is the use of the CO_2 yield, which is a single valued measure of how much carbon in the fuel reactor is fully oxidized to CO_2. The CO_2 yield, expressed through γ_{CO2}, does not consider gas leakage from the fuel reactor to the air reactor or transport of solid carbon to the air reactor. Hence, the quantity in reaction (10) can only be called a yield if carbon loss to the air reactor is negligible or exclusively due to gas leakage. Furthermore, it is not differentiated by equation (10) how far fuel is oxidized. The CO_2 yield is expressed as the molar flow of CO_2 that leaves the fuel reactor divided by the sum of all carbon that leaves the fuel reactor. This ratio can be rewritten with concentrations instead of molar flows, see equation (10).

$$\gamma_{CO2} = \frac{\dot{n}_{CO2,FR}}{\dot{n}_{CO2,FR} + \dot{n}_{CO,FR} + \sum_{m=1}^{9}(m \cdot \dot{n}_{CmHn,FR})} = \frac{y_{CO2,FR}}{y_{CO2,FR} + y_{CO,FR} + \sum_{m=1}^{9}(m \cdot y_{CmHn,FR})} \tag{10}$$

Table 2: Overview of CLC and CLOU experiments with manganese-based oxygen carrier M4MZ-1200 (M-series) and copper-based oxygen carrier C2Z-1050 (C-series)

Test number	Fuel flow FR (ml_{liq}/min)	Steam flow FR (ml_{liq}/min)	Steam flow FR (L_n/min)	Air flow AR (L_n/min)	T_{FR} (°C)	H/C (–)	Corresponding power (W)	Operation time (min)
M1	0.25 – 0.80	0.75	0.93	7.0 – 9.0	900	7.7 – 3.7	144 – 462	507
M2	0.25 – 0.80	0.75	0.93	7.0 – 9.0	950	7.7 – 3.7	144 – 462	275
M3	0.25 – 0.80	0.75	0.93	7.0	800	7.7 – 3.7	144 – 462	261
C1	0	0	0	6.0	850 – 975	–	0	200
C2	0.25 – 0.50	0.75	0.93	8.0	800	7.7 – 4.8	144 – 289	237
C3	0.25	0.75	0.93	8.0	850	7.7	144	437
C4	0.25	0.75	0.93	8.0	750	7.7	144	356
C5	0.25	0.75	0.93	8.0	700	7.7	144	81
C6	0.25	0.75	0.93	8.0	650	7.7	144	40
C7	0.25	0.75	0.93	8.0	900	7.7	144	1542
C8	0	0	0	6.0	850 – 975	–	0	126

Table 3: Carbon fate categories

C-Species	Symbol	Explanation
CO_2 in FR	$C_{CO2,FR}$	Reaction product in case of complete oxidation
CO in FR	$C_{CO,FR}$	Intermediate reaction product; hydrocarbons are fully reformed but only partially oxidized
CH_4 in FR	$C_{CH4,FR}$	Intermediate reaction product; hydrocarbons are mostly reformed but not fully oxidized
$>CH_4$[a] in FR	$C_{>CH4,FR}$	Intermediate reaction product; hydrocarbons are not or partially reformed
CO_2 in AR	C_{AR}	All carbon that gets into the air reactor is expected to be fully oxidized to CO_2. Carbon can either get into the air reactor in the form of gas, *i.e.* by gas leakage from fuel reactor to air reactor, or as solid carbon from coke formation, which is transported into the air reactor by the global particle circulation. However, it is only possible to observe the sum of both effects.

[a] $>CH_4$ denotes hydrocarbons higher than CH_4

3.2. Oxygen Carrier

One way to characterize an oxygen carrier is through the oxygen transfer capacity, R_o, which depends on type and ratio of active and inert phase. It expresses the highest theoretic mass change between the state of complete oxidization, $m_{OC,ox}$, and full reduction, $m_{OS,red}$, see equation (11).

$$R_o = \frac{m_{OC,ox} - m_{OC,red}}{m_{OC,ox}} \tag{11}$$

The actual oxygen carrier reduction can be described through the degree of oxidation, X, see equation (12), and the degree of mass-based conversion, ω, see equation (13).

$$X = \frac{m_{OC} - m_{OC,red}}{m_{OC,ox} - m_{OC,red}} \tag{12}$$

$$\omega = \frac{m_{OC}}{m_{OC,ox}} \tag{13}$$

The current mass of the oxygen carrier, m_{OC}, cannot be determined explicitly during operation of the 300 W reactor. Hence, the only way to ascertain the actual degree of reduction is to indirectly infer it from how much oxygen is needed to oxidize the oxygen carrier after the fuel flow is shut off. This so called reoxidation is usually performed at the end of each experiment.

It is possible to calculate the oxygen carrier circulation, $\dot{m}_{OC}$, see equation (14), as a function of ω, the oxygen consumed in the air reactor, $\Delta\dot{m}_{O2,AR}$, and the degree of mass-based conversion in the air reactor, ω_{AR}. Here, ω is derived from reoxidation data, see equation (13), and $\Delta\dot{m}_{O2,AR}$ from continuous operation. If it is assumed that the oxygen carrier is completely oxidized in the air reactor, then ω_{AR} in equation (14) becomes 1. Hence, the oxygen carrier circulation can be estimated for the experimental conditions used prior to reoxidation.

$$\dot{m}_{OC} = \frac{\omega_{AR} \cdot \Delta\dot{m}_{O2,AR}}{\Delta\omega} = \frac{\cancelto{1}{\omega_{AR}} \cdot \Delta\dot{m}_{O2,AR}}{\cancelto{1}{\omega_{AR}} - \omega} \tag{14}$$

The average attrition rate was calculated from a simple exponential decay equation, based on the experimental time with fuel addition, the amount of recovered fines and the total recovered bed mass. Particles are hereby assumed to decay evenly over the whole experiment time, which is a simplified assumption. Here, fines are defined as particles with a diameter less than 45 µm.

4. Results and Discussion

4.1. Fuel Combustion with M4MZ-1200

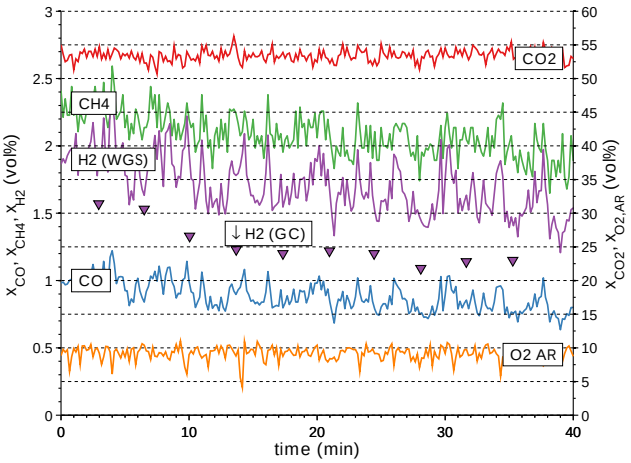

Figure 5: Dry-gas concentrations during chemical-looping combustion with M4MZ-1200 at T_{FR} = 900 °C with 289 W_{th} (0.5 ml_{liq}/min) fuel and 0.75 ml_{liq}/min steam (H/C = 5.1). The balance is argon, which was used to fluidize the loop-seals and about 4 % of nitrogen, which leaked from air reactor to fuel reactor. The wet flue gas consisted of about 60 % steam. The AR was fluidized with 7.0 L_n/min air.

Figure 5 shows dry-gas concentrations measured during experiment M1 with 289 W_{th} fuel equivalent, *cf.* Table 2. The concentration of hydrogen, H2 (WGS), is 1.7 % on average and was calculated under the assumption that the equilibrium of the water-gas shift reaction is valid. The validity of this assumption is confirmed by gas chromatograph measurements, H2 (GC), which are about 0.4 %-points lower. Argon was used during all experiments to fluidize the loop-seals. The measured dry-gas concentration of nitrogen in the fuel reactor, which is a result of minor leakage from air reactor to fuel reactor, varied between 1 % and 4 % in the experiments.

About half of the oxygen provided by the air flow in the air reactor was transported into the fuel reactor. For an industrial CLC unit, almost all the oxygen should be used so that only a few percent remain in the exhaust gases of the air reactor. The average concentrations of CH_4 and CO are 2.1 % and 0.9 % respectively.

Figure 6 shows the carbon conversion during the experiments. The temperature was varied between 800 °C and 950°C for each fuel flow.

The following can be seen in Figures 6a – 6c:

- Higher temperatures lead to a lower content of CH_4 and other hydrocarbons.
- The amount of fully converted CO_2 and the CO_2 yield increase with higher temperatures.

The CO_2 yield reaches a maximum of 99.3 % and a minimum of 83 % in the temperature interval investigated. The fraction of unconverted H_2 was in the same order of magnitude as the CO concentration, which was clearly below 1 % at all times.

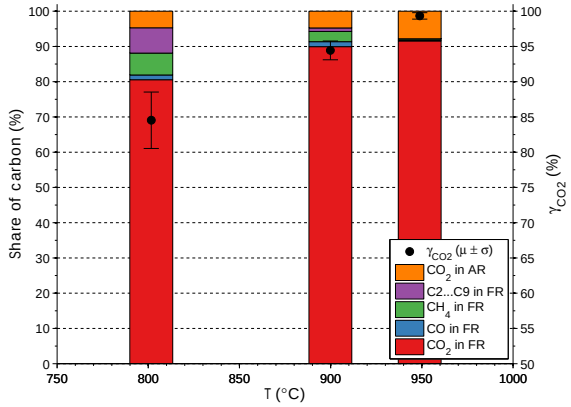

(a) 144 W_{th} (0.25 ml_{liq}/min)

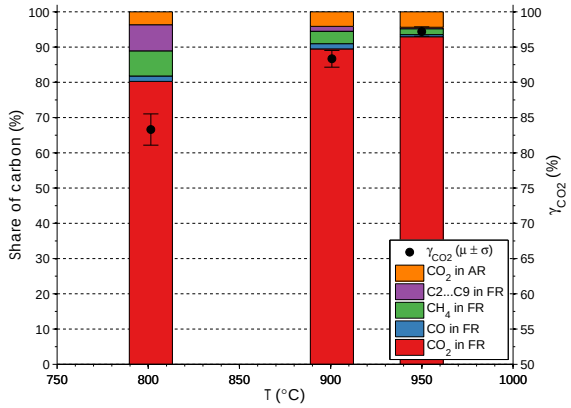

(b) 289 W_{th} (0.50 ml_{liq}/min)

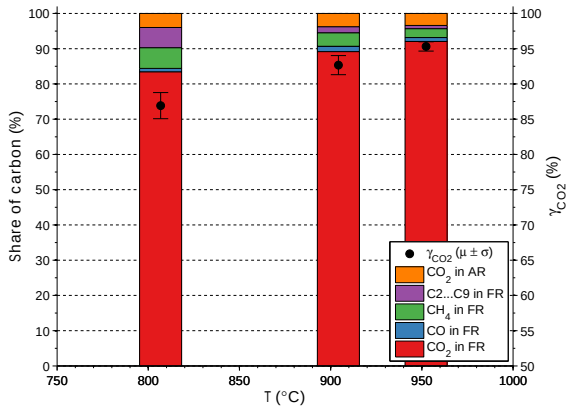

(c) 462 W_{th} (0.80 ml_{liq}/min)

Figure 6: Carbon fate and CO_2 yield for CLC experiments with M4MZ-1200 for different fuel flows and temperatures

The fraction of carbon transported to the air reactor lies between 3 % and 9 %.

Higher temperatures benefit both hydrocarbon decomposition and reaction kinetics. This explains the observations made, *i.e.* improved fuel conversion at higher temperatures, and matches earlier results with a similar oxygen carrier and natural gas as fuel [17, 23].

A variation in air flow, which is believed to affect the circulation of particles, was investigated but only resulted in minute

changes. This indicates that circulation is sufficient and does not limit the performance.

4.2. Fuel Combustion with C2Z-1050

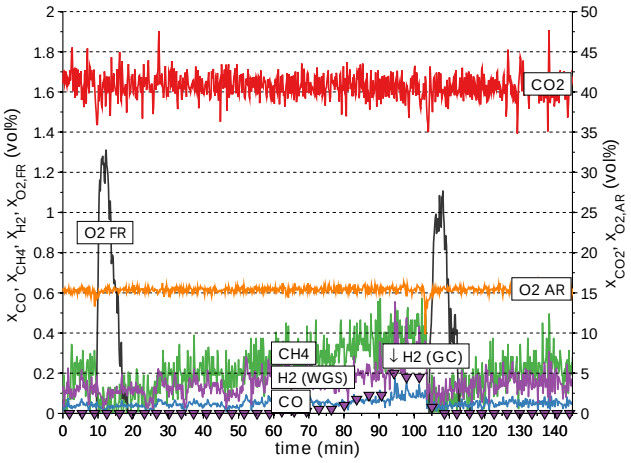

Figure 7: Dry-gas concentrations during chemical-looping combustion with C2Z-1050 at T_{FR} = 900 °C with 144 W_{th} (0.25 ml_{liq}/min) fuel and 0.75 ml_{liq}/min steam (H/C = 7.7). The balance is argon, which was used to fluidize the loop-seals and about 1 % of nitrogen, which leaked from air reactor to fuel reactor. The wet flue gas consisted of about 60 % steam. The AR was fluidized with 8.0 L_n/min air.

Figure 7 shows dry-gas concentrations measured during experiment C7 with 144 W_{th} fuel equivalent, *cf.* Table 2. The concentration of hydrogen, H2 (WGS), is about 0.2 % and was calculated under the assumption that the equilibrium of the water-gas shift reaction is established. This assumption can be compared to gas chromatograph measurements, H2 (GC), which showed a concentration of $\ll$ 0.1 % in most cases. The loop-seals were fluidized with argon during all experiments. The measured dry-gas concentration of nitrogen, which is a result of minor leakage from air reactor to fuel reactor, is about 1 % during most experiments.

A little less than 25 % of oxygen added to the air reactor was transported into the fuel reactor. The average concentration of CH_4 is about 0.2 % and the CO concentration is clearly lower than 0.1 %. Fuel conversion to CO_2 and H_2O is nearly complete.

A release of gas-phase oxygen can be seen twice during the operational window shown in Figure 7, starting at about 10 min and 105 min respectively. During operation when no oxygen is detected in the off-gases, the released oxygen is probably consumed by fuel or intermediate reaction products, *e.g.* CO, H_2 or CH_4. The consumption of oxygen by mentioned gases could either occur in the particle bed or in the freeboard, *i.e.* above the bed. It is assumed though that gas-phase oxygen was released continuously by the oxygen carrier.

As can be seen in Figure 7, the concentrations measured oscillate slightly. This is believed to be a result of a somewhat unsteady global particle circulation. It seems like there was a build-up of oxygen carrier in some part of the reactor, which was released in regular intervals and caused an oscillation in fuel conversion.

The oxygen release properties of C2Z-1050 were investigated under continuous circulation of oxygen carrier particles but without fuel addition before and after the combustion experiments, *cf.* Table 2. During those experiments particles in the fuel reactor were fluidized with nitrogen so that released oxygen could be detected. Gas-phase oxygen was found to be released continuously and without noteworthy fluctuations. The results of the oxygen release experiments are shown in Figure 8. For comparison, the equilibrium concentrations of oxygen are included in the figure. It can be seen that the experimental data is close to equilibrium.

Even though gas phase oxygen is released, it is believed that fuel does not exclusively react with released oxygen. Thus, less CLOU and more CLC is expected under conditions when oxygen is not released rapidly enough to convert surrounding fuel, *e.g.* at lower temperature and at high concentrations of fuel as in the bottom zone of the fuel reactor.

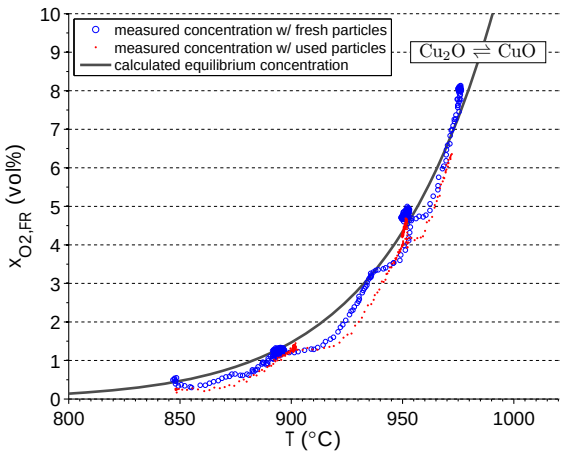

Figure 8: Oxygen release of C2Z-1050 in fuel reactor under continuous particle circulation without fuel addition at different temperatures. Each data point corresponds to a logged value with 10 s between samples.

When the fuel flow was increased, the amount of oxygen entering the fuel reactor with oxygen carrier particles did not increase proportionally, which led to a drastic fall in gas conversion after a few minutes. However, since the experiments with C2Z-1050 were performed at rather low temperatures, the particles did not agglomerate and conversion could be re-established after the fuel flow was reduced to the initial level. The carbon conversion of liquid fuel with varied temperature is shown in Figure 9.

Experiments with C2Z-1050 were run at lower temperatures than experiments with M4MZ-1200. The fuel conversion achieved, however, was higher. The CO_2 yield was above 85 % at all times and higher than 95 % at temperatures above 750 °C. The maximum CO_2 yield of 99.4 % in Figure 9 could be raised to 99.99 % through variation of the air flow and the circulation respectively. At high conversion levels oxygen was detected in the fuel reactor off-gas.

Between 1.2 % and 2.4 % of fuel carbon ended up in the air reactor. The amount of hydrocarbons from the fuel reactor decreases with higher temperature and the dry-gas concentrations

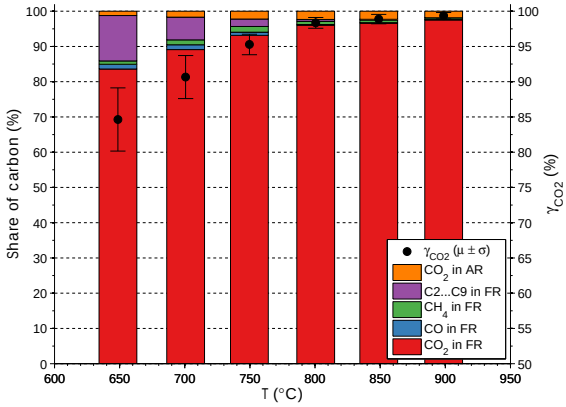

Figure 9: Carbon fate and CO_2 yield for CLC experiments with C2Z-1050 for 144 W_{th} (0.25 ml_{liq}/min) at different temperatures

of CO and CH_4 were below 1 % at all times. The maximum dry-gas concentration of H_2 measured was 4 % at 650 °C, which was the lowest temperature tested. This comparatively high value can be attributed to the water-gas shift reaction, which favours a shift from CO and H_2O to CO_2 and H_2 at temperatures below 800 °C.

The lowest temperatures investigated, 650 – 750 °C, are probably not very realistic, especially for commercial applications. Oxygen release at such temperatures is so low that CLOU properties, which are an important benefit of this material, can be neglected, see Figure 8. However, fuel conversion at such temperatures is still high, which makes the results interesting.

4.3. Carbon Leakage and possible Coke Formation

Carbon leakage from fuel reactor to air reactor was observed for both oxygen carriers tested. Possible mechanisms for this leakage are coke formation on the oxygen carrier and gas leakage, see Table 3, although gas concentrations measured only show the sum of both. There are several facts, which speak for each mechanism.

Thermodynamically, carbon formation with methane as fuel should not be possible when slightly above 25 % of the oxygen needed for combustion is supplied by the oxygen carrier or added steam and the temperatures is above 850 °C [15, 17]. 25 % of the oxygen needed for combustion of methane corresponds to the amount of oxygen needed to convert methane fully to CO and H_2. This means that a small excess of H_2O is sufficient to suppress coke formation. A thermodynamic calculation, which was performed as part of this work, shows that this also applies for hydrocarbon fuels with different hydrogen-to-carbon ratios; if enough oxygen is provided, either by the oxygen carrier or added steam, to convert all C to CO, coke formation does not occur if the temperature is sufficiently high. With more oxygen added the required temperature decreases.

For the fuel used here, the minimum amount of oxygen required to avoid coke formation is approximately 34 % of the stoichiometric amount. The amount of oxygen provided by the steam used in the feeding system corresponds to 100 % of the stoichiometric amount for the lowest fuel flow used, *cf.* M1 – M3 and C2 – C7 in Table 2, and 31 % for the highest fuel flow used respectively, *cf.* M1 – M3 in Table 2. Thus, there was a large excess of oxygen available already from added steam to avoid coke formation except for the highest fuel flow, where it was nearly sufficient. However, with the oxygen carrier present there should always be enough oxygen available to avoid coke formation. Coke formation should not be thermodynamically favoured.

Besides the obvious carbon transport to the air reactor, see Figures 6 and 9, there seems to be no further noteworthy carbon deposition in the fuel reactor during fuel addition. After each experiment the circulation was stopped so that reduced particles stayed in the fuel reactor. When thereupon the particles were reoxidized by air, some CO_2 was detected. This CO_2 corresponded to less than 0.5 % of the total fuel carbon added during the preceding experiment with manganese-based M4MZ-1200 and less than 0.3 % for copper-based C2Z-1050. It should be mentioned that it is not clear whether this carbon was formed on the particles or somewhere else in the fuel reactor, *e.g.* pressure taps, reactor walls, windbox or fuel line.

Carbon leakage has not been observed in larger units with gaseous fuel and nickel-based oxygen carrier, which is known to catalyze coke formation [24–27]. In the 300 W unit however, carbon leakage has been observed with different oxygen carriers and different gaseous fuels. In this reactor, gas leakage from fuel reactor to air reactor is favoured due to a slight overpressure in the fuel reactor compared to the air reactor.

The fact that carbon leakage differed for the oxygen carriers tested, *cf.* Figures 6 and 9, might be an indicator for coke formation on the oxygen carrier. Carbon formation on manganese-based oxygen carrier with methane as fuel has been mentioned in earlier studies [16, 28, 29], whereas oxygen release properties of C2Z-1050 oxygen carrier might have inhibited coke formation on the particles to a large extent.

Carbon formation has often been seen in laboratory tests, where the oxygen carrier may be more or less completely reduced and the fuel goes through the reactor essentially unconverted at the end of a reducing cycle. A dedicated laboratory study of carbon formation with nickel-based oxygen carrier showed that significant carbon formation was seen only when gas conversion was very low, *i.e.* below 10 – 20 % [30].

Coke formation mechanisms could be different for liquid fuels than for gaseous fuel, but no safe conclusions can be drawn at the moment.

4.4. Oxygen Carrier Circulation and Reduction

Based on the oxygen consumption of the reduced particles in the fuel reactor after fuel shut-off, the particle reduction, ω and X, and the global particle circulation were estimated. For both oxygen carrier materials this was done during a number of occasions. The results shown in Table 4 are expressed in the form of mean value plus/minus one standard deviation. The product of $(1 - \omega)$ and $\dot{m}_{OC}$ corresponds to the oxygen that is transported into the fuel reactor. While the degree of mass-based conversion, *i.e.* the reduction, of both materials is similar, the circulation of M4MZ-1200 is clearly higher than that of C2Z-1050. The difference in oxygen carrier circulation seems

to be a result of the difference in bulk density, see Table 5. It becomes clear that the amount of oxygen available in the fuel reactor was much lower for the copper-based oxygen carrier than for the manganese-based oxygen carrier.

4.5. Oxygen Carrier Analysis

During the experiments with M4MZ-1200 a large amount of fines accumulated in the particle filters. The rate of accumulation seemed to be higher during early experiments than during later ones. This could be due to high gas velocities in the fuel reactor. As the fuel flow was raised above the design value of 300 W_{th} and with fuel conversion being nearly complete, the gas flow approached the particles' terminal velocity. This caused not only fines to be blown out of the reactor but also particles of larger size. After 17 h of experiments under fuel addition it was no longer possible to fluidize the oxygen carrier M4MZ-1200.

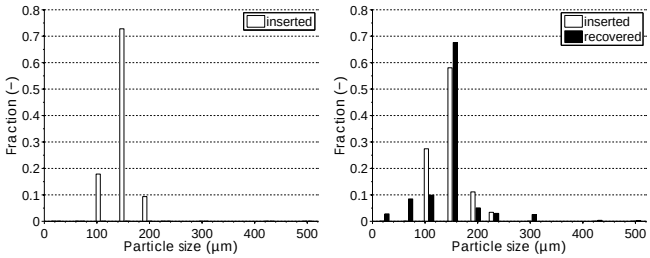

(a) M4MZ-1200 **(b)** C2Z-1050

Figure 10: Particle size distribution of inserted and recovered bed material of (a) manganese-based oxygen carrier (b) copper-based oxygen carrier

When the reactor was opened after the experiments with M4MZ-1200 the appearance of the material had changed considerably. It was no longer pourable and its consistency resembled that of flour. Sieving the material was not possible and thus the particle size fractions were separated through sedimentation, *i.e.* wet sieving. The particles were thereby divided into coarse and fine fractions. The coarse particles were very soft and turned to dust under slightest pressure. After wet sieving, the material was dried in an oven overnight. Nonetheless, after a few days condensate was observed in the closed sample containers. The used manganese material seems to be hydrophilic. Due to the mentioned phenomena a reliable estimation of particle lifetime and attrition rate was difficult to make. The particle size distribution of fresh particles, *i.e.* bed material inserted in the reactor, is shown in Figure 10a.

The disintegration of the whole batch of the manganese-based oxygen carrier material was unexpected. A similar material, which was freeze-granulated and not spray dried, has been used successfully in the 300 W reactor using natural gas and syngas as fuels at flows corresponding to 100 – 300 W for a total of 70 h and temperatures up to 950 °C [17]. The fact that the fuel flow used here was increased up to 462 W_{th} might have caused a significantly higher reduction of the oxygen carrier, which in turn might be the reason for the disintegration of the particles.

A low and constant build-up of fines was observed in the particle filters during 45 h of fuel operation with C2Z-1050 oxygen carrier. Figure 10b shows the particle size distribution of fresh particles, *i.e.* bed material inserted in the reactor, and used particles, *i.e.* bed material that was recovered after the experiments. The amount of fines, *i.e.* particles from recovered bed material, particle filters and water seal with a size below 45 µm, was the basis for an estimation of attrition rate and particle lifetime. The average attrition rate of C2Z-1050 oxygen carrier during fuel operation was 0.25 %/h. In a fluidized bed reactor a constant make-up feed of bed material is usually necessary. The loss of 0.25 %/h would then correspond to a lifetime of 400 h. Long term testing with nickel-based particles showed a significant decrease in attrition rate after 1000 h as compared to the initial 50 – 100 h [24, 25]. Two effects seem likely for high attrition in the first period. Firstly, fragmenting of soft or deformed particles and secondly, abrasion as surface irregularities are abraded off particles. Assuming a similar behaviour of the C2Z-1050 particles it is likely that the average lifetime of the bed material should be considerable larger than 400 h.

When the reactor was opened after the experiments an agglomerated block was noticed in the bottom of the fuel reactor. The agglomerate covered the entire cross-sectional area of the fuel reactor (25 mm × 25 mm) and was about 5 mm high. There were some gas channels in the agglomerated block and a continuous gap along the outer edge. The agglomerate is believed to have formed during experiment C8, see Table 2, which was the concluding CLOU test during the experiment series. As the temperature was raised to 975 °C irregularities in fluidization were observed and it was no longer possible to fluidize the particles properly.

Figure 11 shows scanning electron microscope (SEM) images of the spray-dried manganese-based oxygen carrier M4MZ-1200 before and after the experiments with liquid fuel in the 300 W reactor. Generally, the particles are uniformly spherical, which is typical for spray-dried particles, with some minor defects. These defects include doughnut-shaped particles, lemon-shaped particles and particles with satellites connected to their surface, see Figure 11a. Those particles that did not turn to fines during the experiments with liquid fuel included broken spheres, perforated spheres and were generally porous, see Figure 11b.

The copper-based particles C2Z-1050, see Figure 12, were expected to look similar to M4MZ-1200, since they were also produced by spray-drying. Even though the particles were predominantly spherical, there were much more deficiencies than was the case for M4MZ-1200. The amount of perforations, satellites and other surface agglomerates is clearly higher. After the experiments there were almost no visible satellites, but a lot of particles were broken, see Figure 12b. When looking at the intact, not broken particles it seems like the ratio of spherical particles to doughnut-shaped particles increased over the experiments. In other words, the doughnut-shaped particles were more prone to fragmentation than spherical ones. It was observed that the amount of fines, which accumulated in the particle filters during the first hours of experiments, was high but soon decreased to a lower level. It is thus believed that mainly

Table 4: Circulation and reduction of manganese-based oxygen carrier M4MZ-1200 and copper-based oxygen carrier C2Z-1050

Short name	Reduction		Circulation	
	ω (%)	X (%)	$\dot{m}_{OC}$ (g/s)	G_{OC}[a] (kg/s m^2)
M4MZ-1200	99.5 ± 0.1	83.7 ± 1.9	6.2 ± 1.7	99.5 ± 27.9
C2Z-1050	98.9 ± 0.4	43.0 ± 19.7	1.20 ± 0.58	19.2 ± 9.2

[a] based on the cross-sectional area of the riser section (AR)

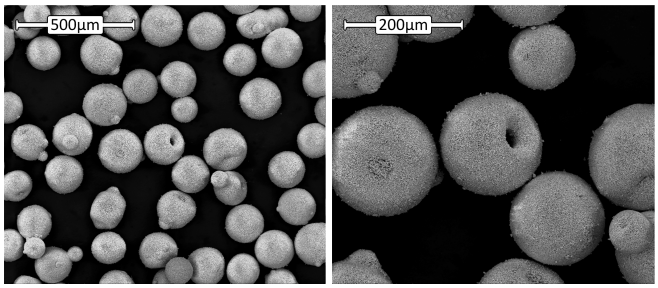

(a) Before experiments

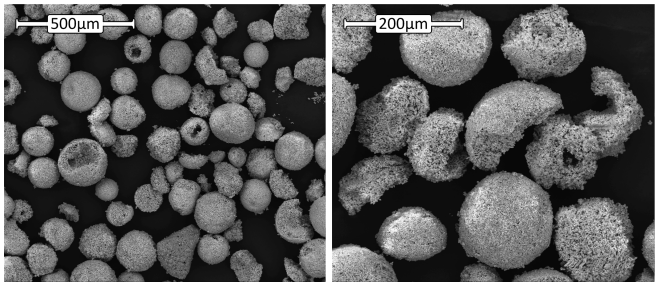

(b) After experiments

Figure 11: SEM images of manganese-based oxygen carrier M4MZ-1200 (a) before and (b) after CLC experiments with liquid fuel

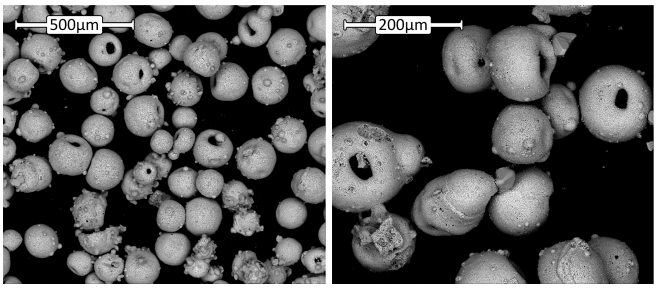

(a) Before experiments

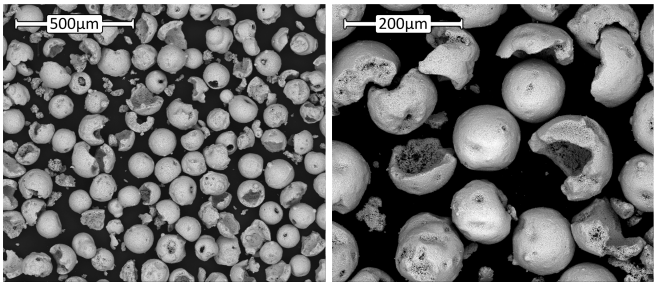

(b) After experiments

Figure 12: SEM images of copper-based oxygen carrier C2Z-1050 (a) before and (b) after CLC experiments with liquid fuel

doughnut-shaped particles fragmented and satellites broke off from the surfaces. After these processes were finished, attrition was mainly dominated by slow abrasion. These observations give additional support to the assumption that the lifetime of bed material should be much longer than 400 h. It should be mentioned that particle fragmentation is not necessarily bad. Particle fragmentation also causes an increase in surface area, which in turn might improve reaction kinetics. Naturally, possible positive effects of fragmentation can only occur if the fragmented particles stay in the particle bed.

Table 5 shows the results of X-ray powder diffractometry (XRD), BET surface area and bulk density of fresh and used M4MZ-1200 and C2Z-1050 particles. The lower detection limit of the XRD analysis lies at about 4 mol%. Here, an exact quantification was not possible. In Table 5, the phases indicated by XRD are listed after occurrence *i.e.* phases with higher intensity are listed first. The BET surface area measurements were performed with nitrogen as adsorbate.

A couple of things should be pointed out with respect to the identified phases. M4MZ-1200 and C2Z-1050 are synthesized oxygen carriers, which are designed so that the active phase, Mn_3O_4 and CuO respectively, are mixed with an inert phase, ZrO_2, in order to increase particle stability and thus lifetime. ZrO_2 has a high thermal resistance and mechanical strength. ZrO_2 undergoes phase changes if temperature is increased. Below 1173 °C it has a monoclinic crystal structure, between 1173 °C and 2370 °C a tetragonal one and between 2370 °C and the melting temperature 2690 °C it becomes cubic [31]. Each crystal structure has a different density, which increases in the order monoclinic → tetragonal → cubic. A phase transformation is thus attended by an abrupt volume change, which is likely to cause cracks in the particle structure. Although the phase transformation temperatures lie well beyond temperatures where chemical-looping experiments are conducted, the initial calcination can well happen in this temperature range, *e.g.* for M4MZ-1200. This means that such particles could a priori have a weakened structure. In order to avoid a phase transformation at high temperatures, ZrO_2 can be stabilized by mixing it with certain metal oxides whose ions diffuse at very high temperatures, about 1700 °C, into the crystal structure of ZrO_2. Such so called stabilized ZrO_2 has a cubic structure at room temperature and does not undergo any structural changes upon heating until the melting point is reached. In order to avoid cracking of particles due to initial heat treatment, it is important that the whole ZrO_2 is stabilized. Such a structure is called fully

Table 5: XRD, BET surface area and bulk density of manganese-based oxygen carrier M4MZ-1200 and copper-based oxygen carrier C2Z-1050

Particles	Indicated phases by XRD	BET surface area (m^2/g)	Bulk density (g/cm^3)
M4MZ-1200			
Before exp. (125 – 180 µm)	ZrO_2 (*m*), Mn_3O_4, Mn_2O_3, ZrO_2 (*c*), ZrO_2 (*t*)	0.6	1.76
After exp. (coarse)	ZrO_2 (*m*), Mn_3O_4, Mn_2O_3, ZrO_2 (*t*), ZrO_2 (*c*)	1.2	0.94
After exp. (fine)	ZrO_2 (m), Mn_3O_4, ZrO_2 (*c*), ZrO_2 (*t*)	–	–
C2Z-1050			
Before (125 – 180 µm)	ZrO_2 (*m*), CuO	0.6	1.54
After (90 – 212 µm)	ZrO_2 (*m*), CuO	0.7	1.68
After (< 90 µm)	ZrO_2 (*m*), CuO	–	–
Agglomerated	CuO, ZrO_2 (*m*), Cu_2O	–	–

(*m*) monoclinic crystal structure (*t*) tetragonal crystal structure (*c*) cubic crystal structure

stabilized ZrO_2 in contrast to partially stabilized ZrO_2. In order to fully stabilize ZrO_2 with MgO, about 15 – 30 mol% MgO have to be mixed with ZrO_2 at high temperatures [32].

M4MZ-1200 consisted of partially stabilized ZrO_2, which means that cubic, tetragonal and monoclinic phases are present, see Table 5. This may be the reason for the high attrition rate of M4MZ-1200. Two solutions are thinkable: either the calcination temperature is reduced to below 1173 °C or fully stabilized zirconium dioxide is used as stabilizing agent. Reducing the calcination temperature might be the easier solution.

C2Z-1050, which consisted of 80 wt% of unstabilized ZrO_2, was sintered at 1050 °C and thus never underwent a phase change. These particles were stable during 45 h of experiments under fuel addition and had a moderate attrition rate. The only noted issue with the copper-based material was that an agglomerate was formed in the bottom of the fuel reactor. XRD of the reoxidized agglomerate showed the presence of copper oxide Cu^{1+} (Cu_2O). Metallic copper (Cu) was not detected within the measuring range. However, this is no evidence that there was no Cu before reoxidation.

The measured BET surface areas of M4MZ-1200 and C2Z-1050 before and after the experiments are generally low. Whereas the BET surface area of M4MZ-1200 doubled over the experiments, that of C2Z-1050 changed only insignificantly, see Table 5. This confirms the aforementioned findings that the structure of M4MZ-1200 undergoes clear changes, whereas C2Z-1050 is mostly stable. The change in surface area for both oxygen carriers seems to match the change in bulk density: whereas M4MZ-1200 undergoes clear changes, only small changes are observed for C2Z-1050, *cf.* Table 5.

5. Conclusions

This paper shows the conversion of kerosene in a chemical-looping process with continuous particle circulation and inherent separation of CO_2. Two oxygen carriers were used; a manganese-based oxygen carrier and a copper-based oxygen carrier, which has the ability to release gas phase oxygen in the fuel reactor.

The following conclusions can be drawn about the manganese-based oxygen carrier M4MZ-1200:

- High fuel conversion was achieved. The CO_2 yield in the fuel reactor was between 83 % and 99.3 % at temperatures between 800 °C and 950 °C and fuel equivalents of 144 – 462 W_{th}.
- Particle attrition was high. At the end of the experiment series it was no longer possible to fluidize the particles as the whole batch of particles was disintegrated. This may be overcome by decreasing the degree of reduction of the particles during fuel combustion.
- The manganese-based material M4MZ-1200 might be suitable for chemical-looping applications if attrition problems can be solved.

The following conclusions can be drawn about the copper-based oxygen carrier C2Z-1050:

- Very high fuel conversion was achieved. With a fuel equivalent of 144 W_{th}, the CO_2 yield in the fuel reactor was above 95 % at temperatures above 750 °C and increased to 99.99 % at 900 °C.
- The amount of fuel that could be converted was limited by the particle circulation.
- The attrition rate was estimated to be 0.25 %/h.
- Agglomeration of the material occurred and probably took place when the temperature was raised to 975 °C.
- The copper-based material C2Z-1050 showed promising results and seems suitable for chemical-looping applications.

Nomenclature

Latin symbols

m	[kg]	mass
$\dot{n}$	[mol/s]	molar flow
$\dot{m}_{OC}$	[g/s]	oxygen carrier circulation
x	[vol%]	dry-gas concentration
y	[vol%]	wet-gas concentration
C	[–]	carbon fraction
G_{OC}	[kg/s m^2]	mass flux of oxygen carrier
H/C	[–]	hydrogen to carbon ratio
R_o	[wt%]	oxygen transfer capacity
S_{BET}	[m^2/g]	BET surface area
T	[°C] or [K]	temperature
T_{boil}	[°C] or [K]	boiling temperature
X	[–]	degree of oxidation

Greek symbols

γ_{CO2}	[%]	CO_2 gas yield
μ	varies	mean value
ρ_{bulk}	[g/cm^3]	bulk density
σ	varies	standard deviation
ω	[%]	degree of mass-based conversion

Indices

$(\,)_{in}$	at the reactor inlet
$(\,)_{ox}$	most oxidized state
$(\,)_{red}$	most reduced state
$(\,)_{AR}$	air reactor
$(\,)_{FR}$	fuel reactor
$(\,)_{OC}$	oxygen carrier

Acronyms

AR	air reactor
C2Z-1050	copper-based oxygen carrier; 20 wt% CuO and 80 wt% ZrO_2 calcined at 1050 °C
CLC	chemical-looping combustion
CLR	chemical-looping reforming
FR	fuel reactor
GC	gas chromatograph
M4MZ-1200	manganese-based oxygen carrier; 40 wt% Mn_3O_4 and 60 wt% MgO-ZrO_2 calcined at 1200 °C
OC	oxygen carrier
SEM	scanning electron microscopy
XRD	X-ray powder diffraction

Acknowledgements

The study is carried out under the project "Chemical-looping with liquid hydrocarbon fuels" financed by Saudi Aramco. The authors would also like to thank Harald Jeppsson from Preem AB for providing the kerosene. A special thanks to Sven-Ingvar Andersson for conduction fuel analysis and helping with his expertise.

References

[1] A. Lyngfelt, B. Leckner, T. Mattisson, A fluidized-bed combustion process with inherent CO_2 separation; application of chemical-looping combustion, Chemical Engineering Science 56 (2001) 3101–3113.

[2] A. Lyngfelt, Oxygen carriers for chemical-looping combustion – 4000 h of operational experience, Oil & Gas Science and Technology 66 (2) (2011) 161–172.

[3] P. Pimenidou, G. Rickett, V. Dupont, M. Twigg, Chemical looping reforming of waste cooking oil in packed bed reactor, Bioresource Technology 101 (16) (2010) 6389–6397.

[4] P. Pimenidou, G. Rickett, V. Dupont, M. Twigg, High purity H_2 by sorption-enhanced chemical looping reforming of waste cooking oil in a packed bed reactor, Bioresource Technology 101 (23) (2010) 9279–9286.

[5] Y. Cao, B. Lia, H.-Y. Zhao, C.-W. Lin, S. P. Sit, W.-P. Pan, Investigation of Asphalt (Bitumen)-fuelled Chemical Looping Combustion using Durable Copper-based Oxygen Carrier, Energy Procedia 4 (2011) 457–464, greenhouse Gas Control Technologies 10.

[6] A. Forret, A. Hoteit, T. Gauthier, Chemical Looping Combustion Process applied to liquid fuels, in: British – French Flame Days, Lille, France, 37–37, 2009.

[7] A. Hoteit, A. Forret, W. Pelletant, J. Roesler, T. Gauthier, Chemical Looping Combustion with Different Types of Liquid Fuels, Oil & Gas Science and Technology – Rev. IFP Energies nouvelles 66 (2) (2011) 193–199.

[8] T. Mendiara, J. M. Johansen, R. Utrilla, P. Geraldo, A. D. Jensen, P. Glarborg, Evaluation of different oxygen carriers for biomass tar reforming (I): Carbon deposition in experiments with toluene, Fuel 90 (3) (2011) 1049–1060.

[9] P. Moldenhauer, M. Rydén, T. Mattisson, A. Lyngfelt, Chemical-looping combustion and chemical-looping reforming of kerosene in a circulating fluidized-bed 300 W laboratory reactor, International Journal of Greenhouse Gas Control 9 (2012) 1–9.

[10] T. Mattisson, H. Leion, A. Lyngfelt, Chemical-looping with oxygen uncoupling using CuO/ZrO_2 with petroleum coke, Fuel 88 (4) (2009) 683–690.

[11] T. Mattisson, E. Jerndal, C. Linderholm, A. Lyngfelt, Reactivity of a spray-dried NiO/$NiAl_2O_4$ oxygen carrier for chemical-looping combustion, Chemical Engineering Science 66 (20) (2011) 4636–4644, ISSN 00092509.

[12] A. Lyngfelt, T. Mattisson, Trestegsförbränning för avskiljning av koldioxid, (Swedish patent application), 2006.

[13] T. Mattisson, A. Lyngfelt, H. Leion, Chemical-looping with oxygen uncoupling for combustion of solid fuels, International Journal of Greenhouse Gas Control 3 (1) (2009) 11–19.

[14] M. Rydén, A. Lyngfelt, T. Mattisson, $CaMn_{0.875}Ti_{0.125}O_3$ as oxygen carrier for chemical-looping combustion with oxygen uncoupling (CLOU) — Experiments in a continuously operating fluidized-bed reactor system, International Journal of Greenhouse Gas Control 5 (2) (2011) 356–366.

[15] E. Jerndal, T. Mattisson, A. Lyngfelt, Thermal analysis of chemical-looping combustion, Chemical Engineering Research and Design 84 (9) (2006) 795–806.

[16] M. Johansson, T. Mattisson, A. Lyngfelt, Investigation of Mn_3O_4 with stabilized ZrO_2 for chemical-looping combustion, Chemical Engineering Research and Design 84 (9 A) (2006) 807–818.

[17] A. Abad, T. Mattisson, A. Lyngfelt, M. Rydén, Chemical-looping combustion in a 300 W continuously operating reactor system using a manganese-based oxygen carrier, Fuel 85 (9) (2006) 1174–1185.

[18] P. Cho, T. Mattisson, A. Lyngfelt, Comparison of iron-, nickel-, copper-, and manganese-based oxygen carriers for chemical-looping combustion, Fuel 83 (2004) 1215–1225.

[19] M. Johansson, Screening of oxygen-carrier particles based on iron-, manganese-, copper- and nickel oxides for use in chemical-looping technologies, Ph.D. thesis, Chalmers University of Technology, Göteborg, Sweden, 2007.

[20] C. Forero, P. Gayán, F. García-Labiano, L. de Diego, A. Abad, J. Adánez, Effect of gas composition in Chemical-Looping Combustion with copper-based oxygen carriers: Fate of sulphur, International Journal of Greenhouse Gas Control 4 (5) (2010) 762–770.

[21] A. Abad, I. Adánez-Rubio, P. Gayán, F. García-Labiano, L. F. De Diego, J. Adánez, Demonstration of chemical-looping with oxygen uncoupling (CLOU) process in a 1.5 kW_{th} continuously operating unit using a Cu-

based oxygen-carrier, International Journal of Greenhouse Gas Control 6 (2012) 189–200.

[22] P. Gayán, I. Adánez-Rubio, A. Abad, L. F. De Diego, F. García-Labiano, J. Adánez, Development of Cu-based oxygen carriers for Chemical-Looping with Oxygen Uncoupling (CLOU) process, Fuel 96 (2012) 226–238.

[23] Q. Zafar, A. Abad, T. Mattisson, B. Gevert, M. Strand, Reduction and oxidation kinetics of Mn_3O_4/Mg–ZrO_2 oxygen carrier particles for chemical-looping combustion, Chemical Engineering Science 62 (23) (2007) 6556–6567.

[24] C. Linderholm, A. Abad, T. Mattisson, A. Lyngfelt, 160 h of chemical-looping combustion in a 10 kW reactor system with a NiO-based oxygen carrier, International Journal of Greenhouse Gas Control 2 (4) (2008) 520–530.

[25] C. Linderholm, T. Mattisson, A. Lyngfelt, Long-term integrity testing of spray-dried particles in a 10-kW chemical-looping combustor using natural gas as fuel, Fuel 88 (11) (2009) 2083–2096.

[26] T. Pröll, P. Kolbitsch, J. Bolhàr-Nordenkampf, H. Hofbauer, A Novel Dual Circulating Fluidized Bed System for Chemical Looping Processes, AIChE Journal 55 (12) (2009) 3255–3266.

[27] P. Kolbitsch, J. Bolhàr-Nordenkampf, T. Pröll, H. Hofbauer, Operating experience with chemical looping combustion in a 120 kW dual circulating fluidized bed (DCFB) unit, International Journal of Greenhouse Gas Control 4 (2) (2010) 180–185, the Ninth International Conference on Greenhouse Gas Control Technologies.

[28] Q. Zafar, T. Mattisson, B. Gevert, Integrated hydrogen and power production with CO_2 capture using chemical-looping reforming-redox reactivity of particles of CuO, Mn_2O_3, NiO, and Fe_2O_3 using SiO_2 as a support, Industrial & Engineering Chemistry Research 44 (10) (2005) 3485–3496.

[29] P. Cho, T. Mattisson, A. Lyngfelt, Defluidization conditions for a fluidized bed of iron oxide-, nickel oxide-, and manganese oxide-containing oxygen carriers for chemical-looping combustion, Industrial & Engineering Chemistry Research 45 (3) (2006) 968–977.

[30] P. Cho, T. Mattisson, A. Lyngfelt, Carbon formation on nickel and iron oxide-containing oxygen carriers for chemical-looping combustion, Industrial & Engineering Chemistry Research 44 (4) (2005) 668–676.

[31] D. Marshall, R. Hannink, Ceramics: Transformation Toughening, in: K. H. J. Buschow, R. W. Cahn, M. C. Flemings, B. I. (print), E. J. Kramer, S. Mahajan, , P. V. (updates) (Eds.), Encyclopedia of Materials: Science and Technology, Elsevier, Oxford, 1113–1116, 2001.

[32] T. Etsell, S. Flengas, Electrical Properties of Solid Oxide Electrolytes, Chemical Reviews 70 (3) (1970) 339–376.